THE ASTROPHYSICAL JOURNAL, 219:230–249, 1978 January 1

CONDENSATION IN SUPERNOVA EJECTA AND ISOTOPIC ANOMALIES IN METEORITES

JAMES M. LATTIMER, DAVID N. SCHRAMM,* AND LAWRENCE GROSSMAN†
The Enrico Fermi Institute, University of Chicago
Received 1977 April 13; accepted 1977 June 17

ABSTRACT

Some of the observed isotopic anomalies in meteorites may be due to presolar grains that originated in supernova explosions. This hypothesis is investigated by performing chemical equilibrium condensation calculations with pressures and compositions that may be appropriate to cooling supernova ejecta. The presupernova star is assumed to have an "onionskin" appearance, the different layers being due to the successive static nuclear burning stages. During the supernova explosion each of these layers undergoes explosive nucleosynthesis. The resulting chemical and isotopic compositions of each layer are discussed. Chemical condensation calculations are then performed for each layer, for several different values of the total pressure, the C/O ratio, and, for the explosive oxygen-burning shell, the (S + Si)/O ratio. It is shown that large (twelve orders of magnitude) changes in the pressure do not significantly affect the condensation sequence, although the equilibrium sequence is shifted in temperature by more than a factor of 2. A scenario is described that attempts to explain the observed isotopic anomalies in oxygen, magnesium, neon, and xenon. Four components of the presolar nebula are considered: interstellar gas and dust (enriched by supernovae throughout galactic history) and "last-event" gas and dust produced by a supernova which occurred about 10^6 yr before the meteorites solidified. This supernova may be necessary to explain the ^{26}Mg anomaly. Only minerals that are stable in the physical environment of the presolar nebula can survive. Type 3 carbonaceous chondrites contain Ca-rich inclusions possessing oxygen and magnesium isotopic anomalies. In their nebular formation regions, only grains of Al_2O_3, $CaTiO_3$, $Ca_2(Al_2, MgSi)SiO_7$, $MgAl_2O_4$, and $CaMgSi_2O_6$ could be presolar in origin. Similarly, enstatite chondrites, which apparently formed in regions of the solar nebula in which C/O > 1, could contain presolar grains of TiC, C, SiC, Fe_3C, AlN, and CaS. All the minerals in these two groups can be condensed in at least one shell of the supernova ejecta model we consider. Possible correlations among both the anomalies observed at present and the anomalies predicted from this investigation are discussed. The correlations of the magnesium and oxygen anomalies with the minerals in which they have been experimentally isolated are examined, and it is shown that the partial melting of Ca-rich inclusions during their formation is consistent with the observations. The four-component scenario may account for the apparent discrepancy in the elapsed time from nucleosynthesis to condensation inferred from magnesium (10^6 yr) and xenon (10^8 yr) isotopic measurements. The lack of anomalies in Ca and Os may indicate that the last-event supernova did not synthesize anything beyond explosive carbon burning, or that matter interior to this zone did not enter the presolar nebula.

Subject headings: abundances — meteors and meteorites — nebulae: supernova remnants — nucleosynthesis

I. INTRODUCTION

Several years ago, Hoyle and Wickramasinghe (1970) suggested that grains might condense in the expanding ejecta from a supernova explosion. Black (1972), Clayton, Grossman, and Mayeda (1973), Eberhardt (1974), Clayton (1975*a*), and Cameron and Truran (1976) have further proposed that such presolar grains may be responsible for the observed isotopic anomalies in meteorites of oxygen, magnesium, neon, and xenon. This paper examines the physical and chemical conditions in an expanding supernova envelope, investigates the likelihood of grain formation, and computes the chemical compositions of these grains. It is then possible to predict what isotopic anomalies one would expect, and further, in what mineral species one ought to observe them. It should be remembered that at the present time there is no observational evidence either way for grain formation in supernova ejecta. Owing to the large distances of extragalactic supernovae, the infrared flux expected from grains may be too small to observe at present.

Clayton *et al.* (1977) presented evidence showing that a component containing nearly pure ^{16}O is present in greater concentrations in the spinel and

* Also Department of Astronomy and Astrophysics, University of Chicago.
† Also Department of Geophysical Sciences, University of Chicago.

pyroxene than in the melilite of high-temperature condensate inclusions in the Allende meteorite. This may be explained in terms of the condensates predicted in supernova ejecta, as we show below. Eberhardt (1974) correlated the Ne-*E* anomaly with a low-condensation-temperature claylike mineral in type 1 carbonaceous chondrites. The excess ^{22}Ne could have originated from ^{22}Na which formed in explosive helium burning and condensed within a few half-lives (2.6 yr) thereafter. For the anomaly to have remained intact in the early solar nebula, the host phase must not have experienced high temperatures or the trapped Ne would have escaped. But, from mineralogical, textural, and chemical considerations, Grossman (1975) argued that C1 chondrites formed in a nebular region in which the temperatures never exceeded 400 K. Another possible explanation for the production of ^{22}Ne lies in intense irradiation in the early solar nebula (Black 1972). Recently, Gray and Compston (1974) and Lee and Papanastassiou (1974) found magnesium isotopic anomalies in Ca-rich inclusions in the Allende meteorite. Lee, Papanastassiou, and Wasserburg (1977) found that the ^{26}Mg/^{24}Mg correlates with the Al/Mg ratio for four coexisting phases (anorthite, spinel, melilite, and fassaite). This is consistent with the interpretation that the ^{26}Mg resulted from the decay of ^{26}Al (7×10^5 yr half-life) after the ^{26}Al was incorporated into the inclusions.

For simplicity, it is assumed that the presupernova star is composed of separate shells which contain the products of the various successive stages of nucleosynthesis in the star. Thus the outer layer should be solar in composition, while subsequent interior shells are composed of the products of normal static hydrogen, helium, carbon, oxygen, and silicon burning (Arnett and Schramm 1973; Arnett 1977). The shock wave resulting from the supernova explosively burns and ejects each layer as it passes through. If it is assumed that no mixing between adjacent layers occurs, then the composition of each shell will not change as the matter expands and cools. Depending on whether the shock wave heats the matter sufficiently to put it in the radiation-dominated region of the (ρ, T)-diagram, a large range in densities can be envisaged for the matter when it has cooled to a few thousand kelvins. If chemical equilibrium is assumed, the condensation temperature varies only slowly with the density, and the condensation sequence is relatively unaffected. However, the validity of the equilibrium approximation depends on the density; it is more valid for higher densities. Furthermore, if the matter does not expand adiabatically, but has a source of heat (radioactivity, for example), the density may become so low by the time the gas has cooled to typical condensation temperatures that condensation may never occur. The supernova model, the composition of the ejecta, and possible trajectories of the cooling matter in the (ρ, T)-plane are discussed in § II.

In § III the chemical equilibrium condensation calculation is described. In § IV, condensation calculations are carried out for a range of chemical compositions and pressures encompassing those deemed possible in § II. In § V, the isotopes that are produced, and those that are left over, in each of the explosive burning zones of a supernova, are discussed. A scenario is developed in § VI for the condensation of the solar system which encompasses all the possible components of pre–solar-system material. These include interstellar gas and dust which have been enriched by supernova explosions throughout galactic history, and gas and dust produced in a last nucleosynthetic event (one or more supernovae). The latter appears to be necessary to explain the ^{26}Mg anomaly (Lee, Papanastassiou, and Wasserburg 1977). The mineralogical character of the possible presolar carrier of isotopic anomalies are then deduced, and the correlation of different anomalies to be expected in these carriers are listed. In § VII, the observed isotopic anomalies in oxygen, magnesium, neon, and xenon are interpreted in terms of this scenario.

II. PHYSICAL AND CHEMICAL CONDITIONS IN SUPERNOVA EJECTA

It is currently thought (see Arnett and Schramm 1973; Schramm and Arnett 1975) that most stars more massive than 6 $M_\odot$ eventually become supernovae. Also, as a result of the successive evolutionary nuclear burning stages, the massive presupernova star may consist of concentric spherical shells, containing unburned fuel in the outermost zone and products of static H, He, C, O, and Si burning in progressively deeper interior zones (Arnett and Schramm 1973; Arnett 1977). When the star becomes a supernova, a shock wave moves out from the core and passes through the mantle and envelope (Falk and Arnett 1977; Chevalier 1976). The passing shock wave heats and explosively burns the contents of each zone (Schramm and Arnett 1975; Hainebach, Norman, and Schramm 1976). The degree of processing may differ from star to star. In fact, in some stars, no significant explosive burning may occur at all. However, the most complete estimates of the composition of supernova ejecta are given by explosive burning calculations. We assume the ejecta to consist of successive zones with compositions corresponding to the explosive burning of hydrogen and the products of normal, static, H, He, C, and O burning. In this paper, these zones will be referred to as the (H), (He), (C), (O), and (Si) zones, respectively. The C/O ratio in the (C) zone decreases with the mass of a star (Arnett and Schramm 1973; Hainebach, Norman, and Schramm 1976). For stellar masses greater than 10–12 $M_\odot$, it becomes less than unity. The chemistry depends mostly on whether the ratio is greater or less than unity—not on its actual value (Larimer 1975; Larimer and Bartholomay 1976). This is due to the stability of the gaseous molecule CO: if C/O > 1, then virtually all the oxygen is bound in CO; similarly, all the carbon is bound if C/O > 1. An exception to this general rule lies in the solar composition case at pressures in excess of 100 atm. Methane becomes more stable than CO and the sequence is independent of the C/O ratio. Furthermore, the C/O ratio in all zones except

TABLE 1

ASSUMED FRACTIONAL NUMBER ABUNDANCES OF THE ELEMENTS

	Zone								
	Solar*		(H) and (He)		(C)		(O)		
Element	O-rich	C-rich	O-rich	C-rich	O-rich	C-rich	S-, Si-poor	S-, Si-rich	(Si)
Al.....	2.5 (−6)	2.5 (−6)	8.3 (−6)	8.3 (−6)	2.3 (−3)	2.3 (−3)	8.1 (−5)	8.1 (−5)	0
C.....	3.7 (−4)	1.0 (−3)	1.2 (−3)	3.2 (−3)	3.2 (−1)	6.5 (−1)	0	0	0
Ca.....	2.2 (−6)	2.2 (−6)	7.1 (−6)	7.1 (−6)	3.7 (−5)	3.7 (−5)	5.0 (−2)	5.0 (−2)	3.0 (−2)
Fe.....	2.4 (−5)	2.4 (−5)	8.1 (−5)	8.1 (−5)	3.7 (−4)	3.7 (−4)	6.6 (−4)	6.6 (−4)	7.5 (−1)
Mg.....	3.1 (−5)	3.1 (−5)	1.0 (−4)	1.0 (−4)	2.3 (−2)	2.3 (−2)	1.0 (−4)	1.0 (−4)	0
H.....	9.4 (−1)	9.4 (−1)	0	0	0	0	0	0	0
He.....	6.5 (−2)	6.5 (−2)	9.96 (−1)	9.94 (−1)	0	0	0	0	0
N.....	1.1 (−4)	1.1 (−4)	3.7 (−4)	3.7 (−4)	0	0	0	0	0
Na.....	1.8 (−6)	1.8 (−6)	5.9 (−6)	5.9 (−6)	2.3 (−3)	2.3 (−3)	5.1 (−5)	5.1 (−5)	0
O.....	6.3 (−4)	6.3 (−4)	2.1 (−3)	2.1 (−3)	6.5 (−1)	3.2 (−1)	4.0 (−1)	1.0 (−1)	0
S.....	1.5 (−5)	1.5 (−5)	4.9 (−5)	4.9 (−5)	3.7 (−4)	3.7 (−4)	1.8 (−1)	2.8 (−1)	1.0 (−1)
Si.....	2.9 (−5)	2.9 (−5)	9.8 (−5)	9.8 (−5)	6.8 (−3)	6.8 (−3)	3.6 (−1)	5.6 (−1)	1.1 (−1)
Ti.....	8.2 (−8)	8.2 (−8)	2.7 (−7)	2.7 (−7)	1.5 (−6)	1.5 (−6)	2.5 (−6)	2.5 (−6)	5.0 (−4)

* Cameron 1973.

the (O) and (Si) zones which contain no C can be greater or less than 1, depending on the initial composition of the star.

Table 1 shows the fractional number abundances assumed for the six zones corresponding to solar (Cameron 1973) and explosive H, He, C, O, and Si burning, respectively. For the present calculation, the 12 elements Al, C, Ca, Fe, H, Mg, N, Na, O, S, Si, and Ti are considered. Future calculations will expand this chemical network. Where appropriate, two values of the C/O or (S + Si)/O ratio have been utilized.

The abundances in the (H) zone are assumed to be the same as in the solar case, except that the hydrogen has been nearly totally converted into He. The relative abundances of elements heavier than O are also solar in the (He) zone, since they are not significantly affected by nuclear burning. Explosive He burning (Howard, Arnett, and Clayton 1971) is not very efficient in converting He nuclei into C and O nuclei. Rather, ^{14}N may be extensively burned into heavier nuclei by alpha capture if the temperature reached in this zone is high enough (see § V). Thus the only major chemical difference between the (H) and (He) zone abundances lies in the N abundance. The quantity of heavier elements produced is small compared with their solar abundances. Since N is nearly inert, the condensation sequences for these zones will be very similar. Thus we have assumed the abundances in these zones to be the same.

During explosive carbon burning, elements heavier than Si are not synthesized in significant amounts and their relative abundances are presumed to be solar. The abundances for the lighter elements in this zone have been taken from some typical results of Pardo, Couch, and Arnett (1974). The nitrogen abundance is zero, while the abundances of C, O, Al, Mg, and Na are greatly increased, even though their relative proportions are roughly solar. The assumed abundances for the (O) and (Si) zones are taken from the work of Woosley, Arnett, and Clayton (1973). In the former zone, elements heavier than Ca are not significantly produced and hence have relative solar abundances, while C is no longer present and Al, Mg, and Na are heavily depleted. The dominant species are O, Ca, S, and Si, and two values for the ratio (S + Si)/O are assumed. The (Si) zone is basically iron peak elements; small amounts of Ca, S, and Si remain.

It should be noted that the abundances used here are meant to be schematic, considering the uncertainty in this supernova picture. It has been checked that, with the exception of the C/O and (S + Si)/O ratios, variations of 20%–50% in relative abundances do not significantly change our results.

Typical conditions for the explosive burning processes lie near the division between the gas-dominated and radiation-dominated regions of the (ρ, T)-plane. Explosive H burning may have a peak temperature around 10^7 K, He around 10^8 K, and C, O, and Si between 1 and 3×10^9 K. These figures are only approximate, since there is considerable uncertainty in these conditions, as indicated by the different values quoted by different authors.

Some possible cooling paths are explored in the Appendix (see Figs. 1 and 2). As the matter cools, it will initially follow, in general, either the trajectory $\rho \propto T^3$ ($\gamma = 4/3$) if the matter is radiation pressure dominated, Figure 1, or $\rho \propto T^{3/2}$ ($\gamma = 5/3$) if the matter is gas pressure dominated, Figure 2. Assuming the cooling to be adiabatic, a large (up to nine orders of magnitude) difference in the final condensation density may arise, depending on which adiabat the matter follows. The photon diffusion time scale is too large for a significant amount of radiation to leak out and cause nonadiabatic cooling until temperatures near 10^4 K are reached. Below this point the cooling can become more rapid, which is also shown in Figures 1 and 2.

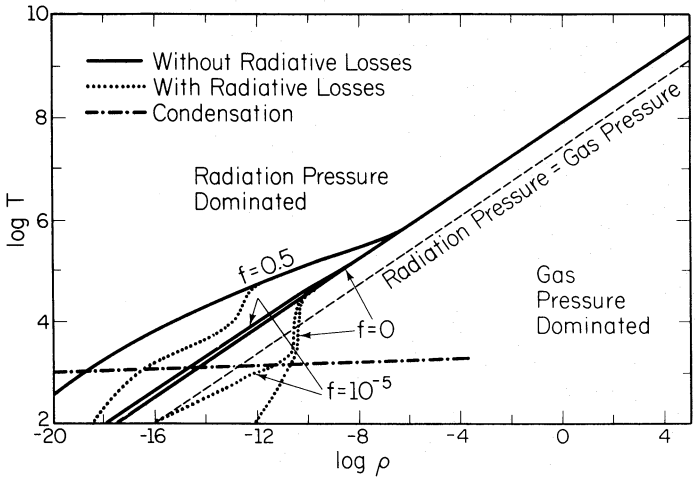

FIG. 1.—Density-temperature diagram showing calculated cooling curves. The initial conditions are $T = 4 \times 10^9$ K, $\rho = 10^5$ g cm^{-3}, $R = 10^8$ cm, and $v = 10^8$ cm s^{-1}, such that the paths lie in the radiation-pressure-dominated region. A dashed line shows the division of the (ρ, T)-plane into a radiation-pressure-dominated part and a gas-pressure-dominated part. The curves are labeled by the parameter f, which is the fraction of the matter initially radioactive. The dotted curves have radiative losses as calculated in the Appendix. Condensation may occur below the indicated dashed line.

The most important nonadiabatic effect on the cooling trajectory may be radioactivity. If a significant fraction by number, f, of the matter is radioactive, the heat input may be sufficient to push a formerly gas-pressure-dominated path over into the radiation-pressure-dominated regime. Even if the path is initially in the radiation regime, the cooling rate may be slowed to such a degree that the condensation density may be lowered by several orders of magnitude from what it would have been in the adiabatic case. The particular case of the (Si) zone, in which ^{56}Ni is formed, is explored in the Appendix and in Figures 1 and 2. It is seen that radioactivity can change the condensation density up to 14 orders of magnitude, perhaps enough to prevent the formation of grains completely. We will defray a discussion of the limiting conditions for grain formation until § IV.

III. THE CHEMICAL EQUILIBRIUM CONDENSATION CALCULATION

The method used to calculate the condensation sequence is essentially that of Grossman (1972), except for two modifications. First, we wish to investigate condensation with the matter cooling adiabatically. Second, the fraction of the total mass that is able to condense may be very large (up to $\frac{1}{2}$ or more), as opposed to the solar case in which most of the matter is hydrogen which does not condense in the region of interest. Thus the pressure cannot be considered a constant, or even a simple function of T.

Chemical equilibrium is assumed among the gas and solid phases. The method employs two principal chemical laws: the conservation of mass and the law

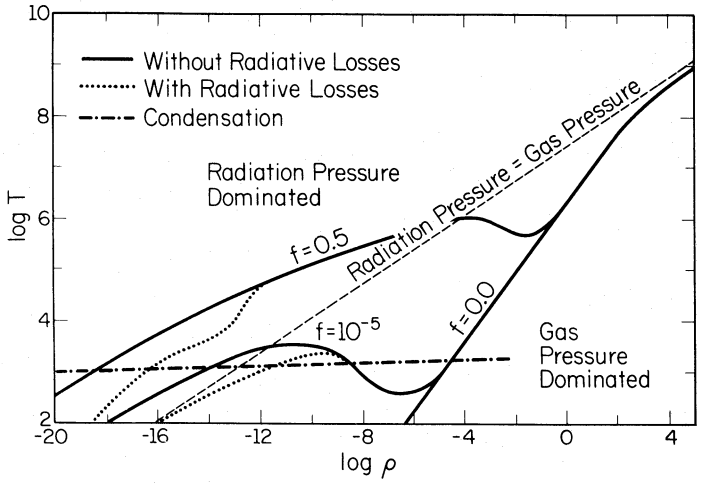

FIG. 2.—Same as Fig. 1 except that all cooling curves have an initial temperature $T = 10^9$ K and therefore lie in the gas-pressure-dominated region.

of mass action. The equation of mass balance for the ith element is:

$$N_i = (V/RT) \sum_j P_j \nu_{ji} + \sum_k S_k \nu_{ki} , \quad (1)$$

where N_i is the total number of atoms of the ith element, P_j is the pressure of the jth gaseous species, ν_{ji} is the stoichiometric coefficient of the ith element in the jth species, S_k is the number of molecules of the kth solid species, V is the volume, R is the gas constant, and T is the temperature. If γ is the adiabatic exponent, then

$$\frac{V}{T} = \frac{V_0}{T_0} \left(\frac{T}{T_0} \right)^{\gamma/(1-\gamma)} , \quad (2)$$

where V_0 and T_0 are the initial volume and temperature. Grossman (1972) essentially used V = constant in place of equation (2), and set the total pressure equal to the pressure of H_2. The appearance of a condensed species k is possible when

$$\prod_i P_i^{\nu_{ki}} \geq A_k/K_k . \quad (3)$$

A_k and K_k are the activity and the equilibrium constant for formation of the solid from the free elements (i), respectively, of the kth species.

These equations are solved by using a Newton-Raphson technique. It is easiest to begin at a temperature sufficiently high that there are no condensed phases. A small error ($\lesssim 5$ K) in the calculation of condensation temperatures is introduced by our procedure of stepping the temperature in finite intervals. We include only species for which known thermodynamic data exist, and which are formed from the 12 elements considered. Table 2 lists these gaseous and solid phases and the sources of their thermodynamic data.

IV. RESULTS OF CONDENSATION CALCULATIONS

In order to have a reference with which to compare our results, Table 3 shows the condensation sequence that Grossman (1972) obtained for the case of solar (C/O = 0.55; Cameron 1968) composition at a pressure of 10^{-3} atm. Compared with this are the results of this paper for the same pressure, assuming no expansion (i.e., $\gamma = \infty$), but with the more recent "solar" composition of Cameron (1973). Melilite is treated as the solid solution of gehlenite ($Ca_2Al_2SiO_7$) and akermanite ($Ca_2MgSi_2O_7$), as is observed in Ca-rich inclusions in the Allende C3 chondrite. In all the

TABLE 2

GASEOUS SPECIES AND SOLID PHASES INCLUDED AND THE SOURCES OF THEIR THERMODYNAMIC DATA

Element	Gases	Solids
Al	AlC, AlH, AlN, AlO, AlOH, AlO_2, AlO_2H, AlS, Al_2O, Al_2O_2	Al, AlN, Al_2O_3, Al_2SiO_5†, Al_4C_3, $Al_6Si_2O_{13}$†
C	CH, CH_2, CH_3, CH_4,* CN, CNH, CNO, CNOH, CN_2, CO, COH, COH_2, COS, CO_2, CS, CS_2, C_2, C_2H, C_2H_2, C_2H_4, C_2N, C_2N_2, C_2O, C_2OH_4, C_3, C_3O_2, C_4, C_4N_2, C_5	C
Ca	CaO, CaOH, $Ca(OH)_2$, Ca_2	Ca, $CaAl_3SiO_6$*†, $CaAl_2Si_2O_8$*†, $CaCO_3$*, $CaMg(CO_3)_2$, $CaMgSi_2O_6$*, CaO, $Ca(OH)_2$, CaS, $CaSO_4$*, $CaSiO_3$*, $CaTiO_3$*, $CaTiSiO_5$*, $Ca_2Al_2SiO_7$*†, $Ca_2MgSi_2O_7$*, Ca_2SiO_4*, $Ca_3Al_2Si_3O_{12}$*†, $Ca_3MgSi_2O_8$*, $Ca_3Mg_5Si_8O_{22}(OH)_2$
Fe	FeO, $Fe(OH)_2$	Fe, FeO, $Fe(OH)_2$, $Fe(OH)_3$, FeS*, $FeSO_4$*, FeS_2*, $FeSiO_3$‡, $FeTiO_3$, Fe_2O_3, $Fe_2(SO_4)_3$*, Fe_2SiO_4*, Fe_3C*, Fe_3O_4
H	HS, H_2,* H_2O,* H_2O_2, H_2S,* H_2SO_4	...
Mg	MgH, MgN, MgO, MgS, Mg_2	Mg, $MgCO_3$, MgC_2, $MgFe_2O_4$, MgH_2, MgO, $Mg(OH)_2$, MgS, $MgSO_4$, $MgSiO_3$, $MgTiO_3$, $MgAl_2O_4$, $MgTi_2O_5$, Mg_2C_3, Mg_2Si, Mg_2SiO_4, Mg_2TiO_4, $Mg_3Si_4O_{10}(OH)_2$, Mg_3N_2
N	NH, NH_2, NH_3,* NO, NOH, NO_2, NO_2H, NO_3, NO_3H, NS, N_2, N_2H_2, N_2H_4, N_2O, N_2O_3, N_2O_4, N_2O_5, N_3	...
Na	NaCN, $Na(CN)_2$, NaH, NaO, NaOH, NaO_2, $Na(OH)_2$, Na_2	Na, $NaAlO_2$, $NaAlSiO_4$*†, $NaAlSi_2O_6$*†, $NaAlSi_3O_8$*†, NaCN, NaH, NaOH, NaO_2, Na_2CO_3, Na_2O, Na_2O_2, Na_2S, Na_2SO_4, Na_2SiO_3, $Na_2Si_2O_5$
S	SO, SO_2, S_2, S_2O, S_8	S
Si	SiC_2, $Si(CH_3)_4$, SiH, SiH_4, SiN, SiO, SiO_2, SiS, Si_2, Si_2N, Si_3	Si, SiC, SiO_2, SiS_2, Si_2, Si_2N_2O§, Si_3N_4
Ti	TiO, TiO_2	Ti, TiC, TiH_2, TiN, TiO, TiO_2, Ti_2O_3, Ti_3O_5, Ti_4O_7

SOURCES.—All data from Joint Army Navy Air Force (JANAF) tables 1960 and later supplements unless otherwise noted.

* From Robie and Waldbaum 1968.

† Robie and Waldbaum 1968 data revised according to Thompson 1974: log K (new) = $(-590/T) \times$ (No. of Al atoms) + log K (old).

‡ From Larimer 1968.

§ From Ryall and Muan 1969.

TABLE 3

"SOLAR"* EQUILIBRIUM CONDENSATION SEQUENCE ($P_{TOT} = 10^{-3}$ atm)

PHASE	TEMPERATURE (Grossman 1972) Appearance	Disappearance	TEMPERATURE (This Work) Appearance	Disappearance
Al_2O_3†	1758	1513	1742	1530
$CaTiO_3$†	1647	1393	1680	1405
Melilite‡	1625	1450	1625	1435
$MgAl_2O_4$‡	1513	1362	1535	1385
(Fe, Ni)*§	1473	...	(Fe)1450	...
$CaMgSi_2O_6$	1450	...	1435	...
Mg_2SiO_4	1444	...	1430	...
Ti_3O_5†	1393	...	1405	1265
$CaAl_2Si_2O_8$*‡	1362	...	1385	1068
$MgSiO_3$	1349	...	1350	...
Ti_4O_7†	...	...	1265	1105
TiO_2	1125	...	1105	760
Al_2SiO_5	...	...	1068	...
$NaAlSi_3O_8$	...	...	1030	780
$NaAlSi_2O_6$	...	...	780	...
$CaTiSiO_5$	...	...	760	...

* Grossman 1972 assumes the abundances of Cameron 1968; this work assumes those of Cameron 1973.

† This work utilizes more recent JANAF thermodynamic data than Grossman 1972.

‡ Robie and Waldbaum (1968) data revised as for Table 2.

§ Grossman 1972 considers the effects of a solid solution of these two elements. This work does not.

tables displayed in this section, the computations were halted, for economy, at the point where the last phase shown condenses; at lower temperatures more phases will condense. The agreement between these calculations, in general, is very good. All of the differences can be accounted for by the explanatory notes in Table 3.

The outermost layer of the presupernova is assumed to have a solar composition. The part of this region that does not undergo explosive processing will have a condensation sequence similar to that of Table 3, except for the effects of expansion and possible variations in the pressure and C/O ratio. Table 4 displays condensation sequences for this "expanding solar" zone, for two initial total pressures, 10^{-3} and 10^{-8} atm, and two C/O ratios, 0.55 and 1.5. The pressure listed in Tables 4–8 is the pressure that would obtain if all atoms were monatomic gases at the temperature at which the first phase condenses. The adiabatic exponent of expansion is now assumed to be 5/3. Thus the pressure is continually decreasing as the temperature is lowered. But the pressure also drops because (1) monatomic gases are consumed as polyatomic gaseous species form, and (2) solid phases condense.

Therefore, near the upper portion of these sequences, the actual total pressure is roughly $\frac{1}{2}$ of the indicated pressure, since most of the atoms are in diatomic species (H_2 and CO), while near the lower end the pressure may be 10 or more times smaller. The effects of expansion can be seen by comparing the nonexpanding solar case (Table 3) with the expanding case (Table 4, C/O = 0.55) for the same total pressure and C/O ratio.

In Table 4, as in the remainder of the tables of this section, the three columns of each sequence list the condensing phases, their condensation temperatures, and the temperatures at which these phases disappear if equilibrium is assumed. If a condensation temperature is higher than the melting temperature for that solid phase, it is underlined. Condensation in the presence of liquids follows a different path and is more complicated because many gaseous compounds will be readily dissolved. Also, the melting points of two coexisting solid phases may be much lower than either of the melting points of the individual solids. We will not further consider the possible effects of liquid phases.

Table 4 shows that, with varying pressure, the relative positions of phases in the condensation sequence usually remain the same. This is true for all compositions considered. Even though the sequences are shifted in temperature by hundreds of degrees when the pressure is changed by several orders of magnitude, the phases which condense, and the order in which they appear, remain largely unchanged. This is beneficial in light of the large uncertainties in our estimates of the pressures. The glaring exceptions to this rule are the condensation points of the pure elements, such as Fe in the low C/O case and C in the high C/O case, relative to other phases.

The changes introduced by varying the C/O ratio are dramatic as long as the total pressure is less than about 100 atm. When C/O < 1, the condensates are silicates, oxides, and metallic iron. But when C/O > 1, carbides, nitrides, and sulfides are the initial condensates. As noted by Larimer (1975), the condensation temperature of the oxides and silicates are

TABLE 4

"EXPANDING SOLAR" ZONE

Phase	T_{cond}	T_{disap}
A. C/O = 0.55		
$P = 2 \times 10^{-8}$ atm		
Al_2O_3	1430	1190
$CaTiO_3$	1350	1129
melilite	1285	1142
$MgAl_2O_4$	1190	1162
$CaAl_2Si_2O_8$	1162	1130
$CaMgSi_2O_6$	1145	760
$MgAl_2O_4$	1131	1090
$CaTiSiO_5$	1129	1124
$MgTi_2O_5$	1124	1096
Mg_2SiO_4	1122	
TiO_2	1096	
$CaAl_2Si_2O_8$	1093	1068
$MgSiO_3$	1086	
Al_2SiO_5	1068	
Fe	1062	
$P = 2 \times 10^{-3}$ atm		
Al_2O_3	1742	1525
$CaTiO_3$	1670	1390
melilite	1622	1419
$MgAl_2O_4$	1525	1360
Fe	1430	
$CaMgSi_2O_6$	1422	
Mg_2SiO_4	1414	
Ti_3O_5	1395	1280
$CaAl_2Si_2O_8$	1360	1068
$MgSiO_3$	1332	
Ti_4O_7	1280	1120
TiO_2	1120	772
Al_2SiO_5	1068	
$NaAlSi_3O_8$	950	780
$NaAlSi_2O_6$	780	
$CaTiSiO_5$	772	
FeS	680	
B. C/O = 1.5		
Phase	T_{cond}	T_{disap}
$P = 2 \times 10^{-8}$ atm		
C	1700	
TiC	1490	
SiC	1310	
Fe	1055	
AlN	1040	897
CaS	1025	
Al_2O_3	894	880
$MgAl_2O_4$	880	784
Mg_2SiO_4	831	
Al_2SiO_5	784	
$P = 2 \times 10^{-3}$ atm		
TiC	1910	
C	1845	
SiC	1730	1044
Fe_3C	1427	1055
AlN	1363	1190
CaS	1353	1026
Al_2O_3	1193	1180
$MgAl_2O_4$	1180	1024
Mg_2SiO_4	1100	
Fe	1055	
$CaMgSi_2O_6$	1044	
Al_2SiO_5	1024	

depressed by several hundred degrees in this case, and iron, at moderate to high pressures, condenses as the carbide Fe_3C. While corundum (Al_2O_3), spinel ($MgAl_2O_4$), diopside ($CaMgSi_2O_6$), forsterite (Mg_2SiO_4), anorthite ($CaAl_2Si_2O_8$), enstatite ($MgSiO_3$), and kyanite (Al_2SiO_5) condense at some pressure no matter what the C/O ratio is; perovskite ($CaTiO_3$) and melilite never condense when C/O > 1 (at less than 10^{-2} atm). This is because Al and Ti condense in the more stable phases, spinel and TiC, before melilite and perovskite condense. It is also notable that when C/O > 1, corundum is stable only over a very small interval (< 20 K). Finally, sulfur condenses at much higher temperatures when C/O > 1, in the form CaS; for C/O < 1, the first sulfide to condense is FeS at about 700 K.

Larimer and Bartholomay (1976) have considered the solar condensation sequence at a constant pressure of 10^{-4} atm for various C/O ratios. Their results for C/O ratios in excess of 1 do not significantly differ from our calculations for the same conditions (not shown).

The next series of sequences, in Table 5, correspond to both the (H) and (He) zones. The differences between the O-rich cases in these zones and in an expanding solar gas (Table 4) are small. They are due to the zero H abundance assumed for the cases illustrated in Table 5. This has two effects: (1) the partial pressure of the remaining elements is substantially increased at the same total pressure, forcing condensation to occur at higher temperatures; and (2) oxygen in excess of CO can no longer form H_2O, increasing the partial pressure of O even more, thus making the gas far more oxidizing than in the case of Table 4. The latter effect causes iron to condense directly as the oxides FeO and Fe_3O_4 instead of metal which forms in the solar case. Also, $FeTiO_3$ is stabilized relative to TiO_2. In fact, FeO is so stable in these model calculations that it will probably enter into solid solution in magnesium silicates at high temperatures, delaying the appearance of a pure oxide. From Table 5, it is also seen that mullite ($Al_6Si_2O_{13}$) and, at low pressure, grossular ($Ca_3Al_2Si_3O_{12}$) are phases which can form in the (H) and (He) zones which could not in the solar case. The coexistence of forsterite and SiO_2 in Table 5 at 10^{-4} atm is due to our use of thermodynamic data for clinoenstatite, the lower-temperature form of $MgSiO_3$. In the temperature range being discussed here, a higher-temperature form prevails whose thermodynamic data, if available, would cause the coexistence of Mg_2SiO_4 and $MgSiO_3$ instead of Mg_2SiO_4 and SiO_2.

There are no significant changes of the C-rich cases in the (H) and (He) zones from the solar case (Table 4), except that the sequences are shifted to higher temperatures at the same total pressure, which is again due to the zero H abundance in Table 5. If nitrogen is significantly depleted in the (He) zone, AlN will not condense.

The results for the explosive carbon-burning zone are displayed in Table 6. Unlike the previous O-rich (C/O < 1) cases, melilite is less refractory than spinel

TABLE 5

(H), (He) ZONES

A. C/O = 0.55		
Phase	T_{cond}	T_{disap}
$P = 10^{-22}$ atm		
Al_2O_3	1346	1157
melilite	1232	1128
$CaTiO_3$	1207	1119
$MgAl_2O_4$	1162	1145
$CaAl_2Si_2O_8$	1145	1118
$CaMgSi_2O_6$	1132	
$CaTiSiO_5$	1119	1112
$MgAl_2O_4$	1118	1077
$MgTi_2O_5$	1112	1085
Mg_2SiO_4	1109	
TiO_2	1085	930
$CaAl_2Si_2O_8$	1079	1071
$Al_6Si_2O_{13}$	1071	1068
$MgSiO_3$	1070	
Al_2SiO_5	1068	
$FeTiO_3$	930	570
FeO	908	
$NaAlSi_2O_6$	720	
FeS	668	
$CaTiSiO_5$	570	
$P = 10^{-4}$ atm		
Al_2O_3	2020	1788
melilite	1867	1617
$MgAl_2O_4$	1791	1629
Mg_2SiO_4	1683	
$CaTiO_3$	1640	1583
$CaAl_2Si_2O_8$	1637	1071
$CaMgSi_2O_6$	1620	
$CaTiSiO_5$	1583	1575
$MgTi_2O_5$	1575	1445
$MgSiO_3$	1545	
$FeTiO_3$	1445	
FeO	1405	
$Al_6Si_2O_{13}$	1071	1068
Al_2SiO_5	1068	
$NaAlSi_3O_8$	1055	775
FeS	978	
$NaAlSi_2O_6$	775	

B. C/O = 1.5		
Phase	T_{cond}	T_{disap}
$P = 10^{-12}$ atm		
C	1590	
TiC	1270	635
SiC	1100	667
Fe	883	
AlN	875	752
CaS	855	
Al_2O_3	752	740
$MgAl_2O_4$	740	655
Mg_2SiO_4	699	632
Al_2SiO_5	667	
MgS	655	
$MgSiO_3$	638	
TiN	635	
$NaAlSi_2O_6$	632	
SiO_2	625	
Fe	600	
$P = 10^{-4}$ atm		
C	2305	
TiC	1805	912
SiC	1620	980
Fe_3C	1324	1055
AlN	1275	1108
CaS	1260	795
Al_2O_3	1108	1095
$MgAl_2O_4$	1095	959
Fe	1055	
Mg_2SiO_4	1033	917
$CaMgSi_2O_6$	980	952
Al_2SiO_5	959	
$MgSiO_3$	948	
MgS	928	860
TiN	912	802
SiO_2	895	890
FeS	890	
Mg_2SiO_4	860	
$NaAlSi_3O_8$	835	775
Ti_4O_7	802	
$CaMgSi_2O_6$	795	
$NaAlSi_2O_6$	775	

in the (C) zone above 10^{-8} atm. At low pressures, the stability regime for melilite breaks into two parts. At higher temperatures melilite is nearly pure gehlenite; the mole fraction that is akermanite is less than 10^{-6}. Diopside supersedes melilite as the temperature is lowered, only to be replaced by melilite (now ~70% akermanite) at still lower temperatures. Merwinite ($Ca_3MgSi_2O_8$), however, almost immediately replaces the melilite. The double stability regime of melilite also occurs in the (H) and (He) zones above 1 atm. Note that in Table 6, independent of the C/O ratio, the large Mg/Si ratio, relative to previous cases, causes forsterite to consume nearly all the Si; $MgSiO_3$ cannot condense, and the excess Mg condenses as MgO. The lower calcium and titanium abundances depress the condensation point of perovskite and other Ca-rich phases (melilite, CaS). Also, no calcium silicates condense in the C-rich cases of Table 6. Finally, sodium condenses as Na_2S and/or Na_2SiO_3 rather than as high-albite ($NaAlSi_3O_8$) as in previous cases.

Moving inward, the next zone is composed of the products of explosive oxygen burning. This zone is mostly Si, S, O, and Ca (Table 1). The condensation sequences for 10^{-4} and 10^{-12} atm are shown in Table 7. Two values of the (S + Si)/O abundance are considered. The chemistry here is such that SiO plays the role that CO played in the previous zones. Considering the S-, Si-poor cases in Table 7, we note the preponderance of Ca-bearing phases among the early condensates and, at high pressures, the absence of corundum and spinel. This is due to the greatly enhanced Ca and diminished Al abundance relative to the low C/O ratio solar case. The enhanced S abundance in the (O) zone is reflected in the appearance of MgS and CaS. The Si/Mg ratio is so high in this zone that SiO_2 forms at a higher temperature than pure

TABLE 6

(C) ZONE

A. C/O = 0.5

Phase	T_{cond}	T_{disap}
$P = 10^{-12}$ atm		
Al_2O_3	1510	1310
melilite	1325	1253
$MgAl_2O_4$	1310	
$CaMgSi_2O_6$	1253	1216
Mg_2SiO_4	1247	
$CaTiO_3$	1219	
melilite	1216	1213
$Ca_3MgSi_2O_8$	1213	690
MgO	1180	
FeO	984	
Ca_2SiO_4	690	
$P = 10^{-4}$ atm		
Al_2O_3	2330	
$MgAl_2O_4$	2150	
melilite	2024	2012
$Ca_3MgSi_2O_8$	2012	690
Mg_2SiO_4	1980	
MgO	1920	
$CaTiO_3$	1751	
FeO	1575	
Na_2SiO_3	1010	
FeS	895	
Ca_2SiO_4	690	

B. C/O = 2

Phase	T_{cond}	T_{disap}
$P = 10^{-12}$ atm		
C	1762	
TiC	1300	654
SiC	1200	760
Al_2O_3	908	815
Fe	906	
CaS	883	
$MgAl_2O_4$	815	
Mg_2SiO_4	770	
MgO	755	590
MgO	746	
Mg_2TiO_4	654	548
Na_2S	590	
$CaTiO_3$	548	
$P = 10^{-4}$ atm		
C	2500	
TiC	1885	1012
SiC	1855	1200
Al_2O_3	1410	1300
Fe_3C	1388	1055
CaS	1330	
$MgAl_2O_4$	1300	
Mg_2SiO_4	1210	
MgO	1183	
MgS	1170	895
Fe	1055	
Mg_2TiO_4	1012	850
Na_2S	899	
$CaTiO_3$	850	
Na_2SiO_3	831	
FeS	700	

TABLE 7

(O) ZONE

A. S-, Si-Rich

Phase	T_{cond}	T_{disap}
$P = 10^{-12}$ atm		
Si	1130	
TiO	990	
CaS	950	
Fe	930	
Al	910	885
melilite	885	859
$Ca_3Al_2Si_3O_{12}$	859	730
$CaSiO_3$	849	734
$CaMgSi_2O_6$	760	694
SiO_2	734	
$CaAl_2SiO_2O_8$	730	715
Al_2SiO_5	715	
$MgSiO_3$	694	
$P = 10^{-4}$ atm		
Si	1840	
CaS	1520	
TiO	1460	
Fe	1400	
Al_2O_3	1364	1360
melilite	1360	1302
$CaAl_2Si_2O_8$	1302	1038
$CaSiO_3$	1290	1130
$CaMgSi_2O_6$	1170	1035
SiO_2	1140	
Al_2SiO_5	1038	
$MgSiO_3$	1035	975
MgS	975	
$NaAlSi_3O_8$	830	

B. S-, Si-Poor

Phase	T_{cond}	T_{disap}
$P = 10^{-12}$ atm		
Al_2O_3	1395	1365
melilite	1365	1096
Ca_2SiO_4	1323	1130
$CaTiO_3$	1294	1075
$CaSiO_3$	1130	
$Ca_3Al_2Si_3O_{12}$	1096	1094
$CaAl_2Si_2O_8$	1094	
$CaTiSiO_5$	1075	
SiO_2	1055	
$CaMgSi_2O_6$	950	
Fe	915	
$P = 10^{-4}$ atm		
Ca_2SiO_4	2130	1781
melilite	1970	1758
$CaSiO_3$	1814	1115
$CaAl_2Si_2O_8$	1758	1023
$CaTiSiO_5$	1688	1360
SiO_2	1675	
Fe	1410	
Ti_2O_3	1360	1220
$CaMgSi_2O_6$	1340	1015
TiO	1220	
Si	1170	
CaS	1125	
Al_2SiO_5	1023	
$MgSiO_3$	1015	965
MgS	965	
$NaAlSi_3O_8$	830	754
$NaAlSi_2O_6$	754	

magnesium silicates and, when one of these becomes stable, it is enstatite rather than forsterite. In fact, the Si/O ratio is so great that metallic Si condenses from the gas after SiO_2 forms. In this model calculation, Fe and Si are predicted to coexist over a wide temperature range. In reality, however, Fe and Si will probably condense together in an alloy. Perovskite does not condense at high pressure; Ti appears in the solids $CaTiSiO_5$, Ti_2O_3, and finally TiO.

The S-, Si-rich cases in the (O) zone are analogous to the previous cases where the C/O ratio is greater than 1. Both are extremely reducing. Because of the absence of C and N from the (O) zone, carbides and nitrides do not form here. Instead, metallic Si and Fe condense which, in reality, will again form a common alloy. Enhanced abundances of Ca and S allow CaS to form at high temperatures and, as in all other reducing gases investigated herein, oxides and silicates appear at lower temperatures than the earliest condensates. As in the S-, Si-poor case, the high Ca abundance causes Ca-silicates to be prominent and the high Si/Mg ratio favors enstatite and SiO_2 rather than forsterite. TiO condenses instead of perovskite.

The final zone to be considered is the (Si) zone, which has large abundances of iron group elements, plus some remaining silicon, sulfur, and calcium. Oxygen, carbon, aluminum, and sodium are no longer present. Calculations for the range $1–10^{-12}$ atm are presented in Table 8. The condensation sequence is unchanged over this range. Given the abundances in Table 1, there is little choice but for metals to condense first and then, for those which form stable sulfides, to do so at lower temperatures by reaction with gaseous sulfur. Here, as in other cases where Fe and Si coexist, alloys are probably formed instead of separate metallic phases.

TABLE 8

(Si) ZONE

Phase	T_{cond}
$P = 1$ atm	
Fe	2970
Si	2420
Ti	2327
CaS	2320
FeS	1170
$P = 10^{-4}$ atm	
Fe	1820
Si	1670
Ti	1620
CaS	1490
$P = 10^{-12}$ atm	
Fe	1089
Si	1083
Ti	1075
CaS	950

We now examine limiting conditions for formation of grains and chemical equilibrium, and look more closely at some factors which may complicate our analysis. For grains to form in expanding supernova ejecta, it is necessary that the nucleation and growth rates of grains be sufficiently rapid. Models of supernova ejecta (Falk and Arnett 1977; Chevalier 1976) indicate that the matter expands with a roughly constant velocity of 100–1000 km s^{-1}, depending on the zone considered. The expansion rate then depends only on the trajectory the matter follows in the (ρ, T)-plane (Figs. 1 and 2). If free expansion with a $\gamma = 5/3$ adiabat is assumed, the expansion time scale (approximately equal to the elapsed time t since the explosion) at the condensation temperature T_{cond} is of the order of $10^3–10^4$ s; with a $\gamma = 4/3$ adiabat, the time scale is about $10^6–10^7$ s. Introducing radioactivity in appreciable amounts will increase these time scales.

The nucleation rate depends primarily on the collision frequency of the nucleating species. The collision rate of a grain with molecules of its own species is

$$\frac{dX}{dt} = Pf\sigma(N_A/2\pi\mu kT)^{1/2}, \tag{4}$$

where P is the pressure, f is the number fraction of nucleating molecules, σ is the cross-sectional area of a grain, μ is the molecular weight of a nucleating molecule, and N_A is Avogadro's number. If every collision leads to grain growth, then $\sigma \sim 7 \times 10^{-16}(1 + X^{1/3})^2$ cm^2. Assuming the matter follows an adiabatic path γ, equation (4) becomes

$$\frac{dX}{dT} \sim 2 \times 10^{11}(1-\gamma)^{-1} f P_{cond}\,(\text{atm})\left(\frac{t_{cond}}{10^7\ \text{s}}\right) \times \left(\frac{\mu}{40}\right)^{-1/2}\left(\frac{T_{cond}}{1500\ \text{K}}\right)^{-3/2} \times \left(\frac{T}{T_{cond}}\right)^{(7-3\gamma)/(6\gamma-6)}(1 + X^{1/3})^2\ \text{K}^{-1}, \tag{5}$$

where the subscript cond indicates conditions when equilibrium condensation begins. Letting $X = 0$ when $T = T_{cond}$, the integration of equation (5) gives the number of collisions occurring between T_{cond} and a final temperature T_f:

$$X(T_f) \sim 2 \times 10^{44}\left[(1+3\gamma)^{-1} f P_{cond}\,(\text{atm})\left(\frac{t_{cond}}{10^7\ \text{s}}\right) \times \left(\frac{\mu}{40}\right)^{-1/2}\left(\frac{T_{cond}}{1500\ \text{K}}\right)^{-1/2} \times \left(1 - q^{(3\gamma+1)/(6\gamma-6)}\right)\right]^3, \tag{6}$$

using $q = T_f/T_{cond}$. $X(0)$ is thus the maximum size that a grain may attain. Inversion gives the minimum pressure needed to grow a grain of size $X(0)$ if

$T_{cond} \sim 1500$ K, $t_{cond} \sim 10^7$ s, and $\mu \sim 40$:

$$P_{min} \sim 1.5 \times 10^{-15}(1 + 3\gamma)X(0)^{1/3}f^{-1} \text{ atm}. \quad (7)$$

Suppose that $X(0) \sim 10^3$ is a minimal estimate for the size of a presolar grain. Since f is generally less than 10^{-3}, $P_{min} \sim 10^{-10}$ atm, which corresponds to a density of $\sim 10^{-15}$ g cm^{-3}. This estimate has only a small dependence on γ. Nucleation, however, may occur only when the pressure is much greater than P_{min}. Thus, the formation of grains appears doubtful if the trajectory of the cooling matter lies in the radiation-dominated region of the (ρ, T)-diagram. When the matter cools to about 10^4 K, however, luminosity losses may cool the matter rapidly enough compared with the pressure change to initiate condensation in this case (see Fig. 1). But other nonadiabatic effects, such as heating from the central remnant via high-energy particles (cosmic rays) or ultraviolet radiation, and radioactivity, may be important in changing these trajectories and the estimate of P_{min} in equation (7).

Falk and Scalo (1975) have investigated the survival in the postexplosion supernova environment of grains existing before the explosion. Considering the uncertainty in the physical conditions of a supernova envelope and in the optical properties of small grains, they conclude that radiative evaporation will destroy grains that are not extremely transparent in the ultraviolet. In our case, however, this destruction mechanism is not important because this background radiation field is sufficiently diluted by the time condensation temperatures are reached (10^6–10^7 s). The most important destruction processes are collisional evaporation of grains by inelastic collisions with gas particles and sputtering. An analysis similar to that of Falk and Scalo (1975) implies that, even in the presence of a strong radiation field, grains containing fewer than 10^8 molecules are not destroyed. Critical embryo sizes for nucleation are several orders of magnitude smaller than this.

Homogeneous nucleation may be hindered by the deposition of latent heat which increases a grain embryo's temperature and hence its evaporation rate. The lack of exchange reactions involving H-containing molecules (if the H abundance is small) may be important, since latent heat is efficiently removed by these reactions. However, an application of the Clausius-Clapeyron equation (Kantrowitz 1951) shows that if $f \ll 1$, collisions with species other than nucleating molecules dominate, and latent heat effects may be negligible.

We have ignored the presence of ions because their concentrations are small compared with those needed to change the abundances of the gaseous molecules and to affect the condensation sequences; the presence of ions, rather, will tend to assist nucleation. Ion nucleation may substantially increase nucleation rates in some astrophysical environments such as red giants (see, e.g., Fix 1969), but Salpeter (1974) has argued that the formation of silicate grains via ion nucleation will be unimportant. If the onset of nucleation requires a considerable amount of supersaturation, the validity of the chemical equilibrium hypothesis is in jeopardy and the condensation sequence may be affected. If homogeneous nucleation theory (Feder *et al.* 1966) is assumed, it can be shown that the amount of supercooling needed, using a sticking coefficient of unity and typical thermodynamic quantities for silicates, is

$$\Delta T = T_{cond} - T_{nuc} \sim 0.04\, T_{cond},$$

where T_{nuc} is the temperature of effective nucleation. Thus ΔT is of the order of 50–80 K. Graphite requires a smaller ΔT. In any case, the upper part of the sequence may be altered. Trace minerals such as W, ZrO_2, and Os may still be able to condense above the equilibrium condensation temperatures of the major mineral phases in these sequences, even after considerable supersaturation of the former. After such phases condense, the sequence may then proceed normally, since heterogeneous nucleation is easier and faster than homogeneous nucleation.

It can be seen from the condensation sequences of this section that, generally, the stable temperatures for a phase range from less than 10 to hundreds of degrees. If the stability range is small enough, the amount of that phase that actually condenses may be negligible, since the number of collisions of a condensing species on a grain may be quite small. Equation (5) gives the number of collisions dX occurring in an interval dT. Letting $X \sim 10^4$ be the size of the grain on which the nucleating species is condensing, and assuming the standard values for γ, μ, T_{cond}, and t_{cond}, the pressure required for dX collisions is

$$P \sim 3 \times 10^{-15} dX/(f dT) \text{ atm},$$

which is seen to be more stringent than equation (7). As an example, consider the condensation of corundum in the C-rich (He) zone (Table 5). At low pressures, Al_2O_3 has a stability range of about 10 K. If the nucleation rate depends on the deposition of AlO vapor, than $f \sim 10^{-5}$. If dX is taken to be a minimum of 10^3 atoms of Al_2O_3 per grain, then the pressure must be more than 3×10^{-8} atm. If the sticking rate is less than unity, or the relevant reaction rates are slow compared with a few minutes, the pressure has to be even greater for significant amounts of corundum to condense. Thus chemical equilibrium is valid only when the pressure is much greater than that required for nucleation.

Because the exponent of q in equation (6) is small (3/2 for $\gamma = 5/3$), a lower temperature cutoff in the condensation sequence is ill defined, and condensation, once begun, will continue to rather low temperatures. This results from the fact that the decreasing collision frequency at lower temperatures and pressures is offset by the decreasing cooling rate.

The effect of mixing between the supernova shells has been neglected. The shock wave that explosively burns and ejects the matter certainly causes some mixing between zones. Only a detailed hydrodynamic calculation will determine on what scale mixing

occurs, not only in length, but also in time. It is likely that the Rayleigh-Taylor instability causes "fingers" of hot dense matter to penetrate cooler matter farther out, but it is not yet known if this will lead to fine-scale mixing by the time grains begin to condense. At any rate, mixing between adjacent shells appears much more likely than a thorough mixing of the entire supernova ejecta. If the latter occurred, large amounts of H would be mixed into the interior, causing the condensation sequences to approach solar sequences; ^{17}O and ^{18}O would also mix with oxygen from interior zones, thus reducing the ^{16}O excess in these zones (see § V). Mixing on a smaller scale would not alter the results of this section.

Another effect of mixing is to introduce some radioactivity into zones exterior to the silicon-burning zone. If much of this type of mixing occurs, the formation of grains could be hindered by the resulting heat input.

The chemistry of the condensing species will be affected if the C/O ratio changes as a result of mixing, particularly in zones in which the ratio changes from less than unity to greater than unity, or vice versa. As an example, suppose the (He) zone has a large carbon abundance (because of CNO processing) and the (C) zone has a small carbon abundance. Mixing could increase the C/O ratio in parts of the (C) zone enough to make the condensation proceed according to the C-rich C sequence, while other regions of the (C) zone, unaffected by mixing, would condense according to the O-rich sequence.

V. ISOTOPES PRODUCED IN EXPLOSIVE NUCLEOSYNTHESIS

If grains are formed in the expanding ejecta of supernovae, their chemical and isotopic compositions should reflect the nucleosynthesis that occurred in the explosion. The chemical compositions have been discussed in § II. We now discuss the particular isotopic anomalies that could occur in each of the explosive burning zones (H), (He), (C), (O), and (Si). It is important to remember that the products of an explosive burning stage, say (He), may differ significantly from the products of static He burning.

Explosive hydrogen burning produces mainly ^{4}He, ^{13}C, ^{17}O, ^{14}N, and possibly ^{15}N; ^{16}O and heavier nuclei are probably not affected much by this burning stage. As a result, grains formed in this zone may contain anomalously high ratios of $^{13}C/^{12}C$ and $^{17}O/^{16}O$. The $^{15}N/^{14}N$ value varies with the physical conditions assumed for this process.

Explosive helium burning (Howard, Arnett, and Clayton 1971) produces the nuclei ^{12}C and ^{16}O in small amounts. In addition, ^{14}N is enriched in this zone owing to CNO cycling in previous burning stages. Thus the other isotopes of CNO nuclei may be deficient, compared with solar isotopic compositions. If the peak burning temperature is high enough, the reaction series $^{14}N(\alpha, \gamma)$ $^{18}F(\beta^{+}\nu)$ $^{18}O(\alpha\gamma)$ $^{22}Ne(\alpha n)$ ^{25}Mg may significantly deplete the ^{14}N abundance and give rise to substantial quantities of neutrons which will produce the neutron-rich isotopes of elements with $Z \geq 12$. Because of the particular neutron-capture cross sections involved, ^{25}Mg, ^{36}S, ^{37}Cl, ^{40}Ar, ^{57}Fe, and ^{58}Fe will be the most likely to show anomalously large abundances relative to the other isotopes of these elements. But ^{26}Mg, ^{31}P, and the neutron-rich isotopes of Si, Ca, Sc, and Ti could also show large enrichments. Low peak burning temperatures may result in slightly enhanced amounts of ^{15}N and ^{18}O. One should note that, for isotopes with extremely low abundances, like ^{18}O, small amounts of production could have large effects.

Explosive carbon burning (Arnett 1969; Pardo, Couch, and Arnett 1974; Truran and Cameron 1978) nucleosynthesizes ^{20}Ne, ^{23}Na, ^{24}Mg, ^{25}Mg, ^{26}Mg, ^{26}Al, and ^{27}Al; ^{12}C and ^{16}O are left over, so that the ratios $^{13}C/^{12}C$, $^{17}O/^{16}O$, and $^{18}O/^{16}O$ will approach zero. The magnesium isotopes may be produced in roughly solar ratios, but variations in all directions are possible. The $^{26}Al/^{27}Al$ ratio will be of the order of 10^{-3}. The $^{29}Si/^{28}Si$ and $^{30}Si/^{28}Si$ ratios may show slight enhancements relative to their solar ratios owing to neutron capture. The neutron-rich isotopes of S, Cl, Ar, K, Ca, Ti, and Fe could show large enrichments relative to the neutron-poor ones owing to neutron capture either in this explosive burning phase and/or in the quiescent helium-burning stage that preceded it (Couch, Schmeidekamp, and Arnett 1974; Lamb *et al.* 1977), which is perhaps more likely.

In explosive oxygen burning (Truran and Arnett 1970; Woosley, Arnett, and Clayton 1973), ^{16}O, ^{20}Ne, and ^{24}Mg are left over, and the other isotopes of O, Ne, and Mg will be strongly depleted relative to them compared with solar ratios. The major species that are made are ^{28}Si, ^{32}S, ^{33}S, ^{34}S, ^{36}Ar, ^{38}Ar, ^{40}Ca, ^{42}Ca, and ^{46}Ti, which are synthesized in roughly solar proportions. The relative abundances of the heavier isotopes of S, Ca, and Ti are depleted compared with solar. Neutrons produced here or in the static helium-burning phase may enhance the neutron-rich isotopes of Fe.

Explosive silicon burning (Woosley, Arnett, and Clayton 1973) produces mainly Ti, V, Cr, Mn, Fe, Co, Ni, Cu, and Zn, whose isotopes may have roughly solar proportions; ^{28}Si and ^{32}S are left over, so large depletions in the other stable isotopes of Si and S are to be expected relative to these.

VI. SCENARIO FOR THE FORMATION OF THE SOLAR SYSTEM

We will consider the following scenario of the formation of the solar system. The pre–solar-system material contains four general components (Fig. 3*a*). The first two components, interstellar gas and dust, have been enriched by supernova debris throughout the age of the Galaxy. The time between the passage through the Galaxy of successive density waves, each of which may lead to star formation and hence supernovae, is about 10^{8} yr. Since supernovae occur in massive stars ($M \gtrsim 6$–$8\ M_{\odot}$) whose lifetimes are less than 10^{8} yr, the interstellar gas and dust will have been last enriched by a supernova at about the time $\Delta \sim 10^{8}$ yr before the formation of the solar system.

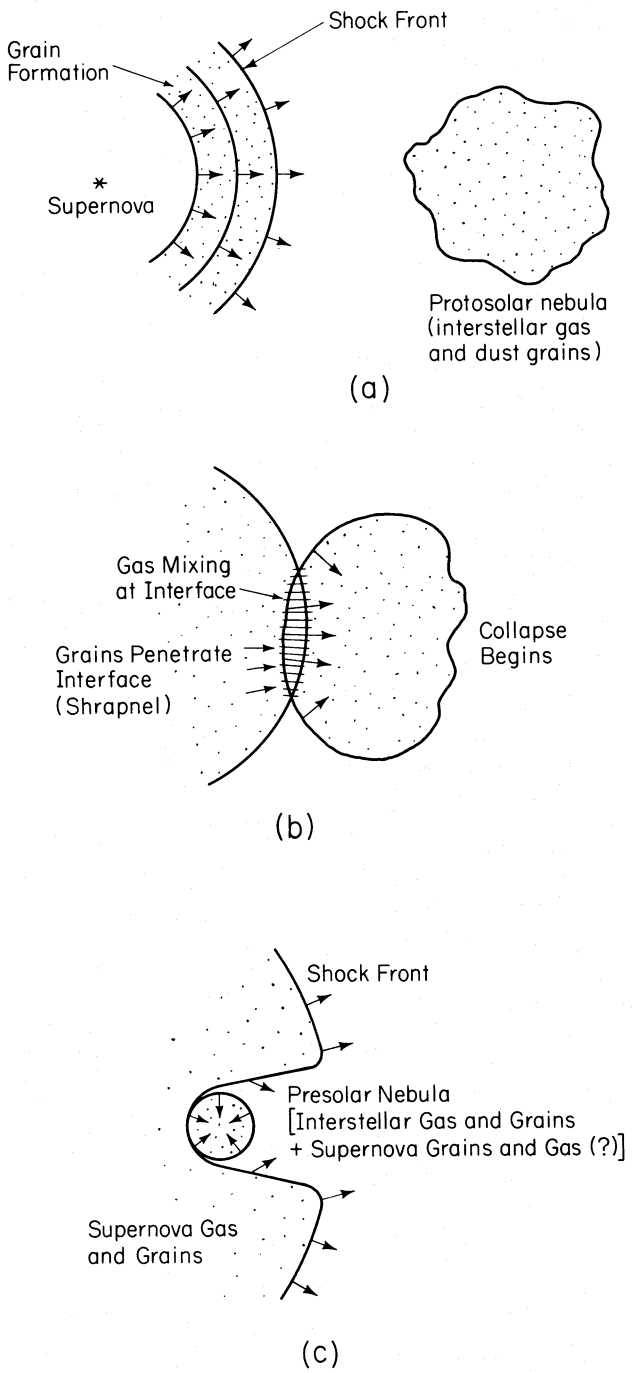

FIG. 3.—Scenario for the formation of the solar system. Fig. 3*a* shows the four components of pre–solar-system material assumed in this paper: Interstellar gas and dust in the protosolar nebula, and supernova gas and dust possibly formed in the expanding supernova ejecta. This ejecta encounters the protosolar nebula and triggers its collapse in Fig. 3*b*. Supernova gas mixes with nebular gas at the collision interface; supernova grains may penetrate into the protosolar cloud. The collapse of the presolar nebula proceeds in Fig. 3*c*. The bulk of the supernova ejecta, continuing to expand, passes around the presolar nebula.

Besides the primary additions of material by supernovae, secondary nucleosynthetic products are continually being added. Among these may be the *s*-process elements, rare CNO isotopes, and the cosmic-ray–spallation-produced nuclei of Li, Be, and B. The interstellar dust component is a heterogeneous mix of all galactic dust. If a substantial fraction of this dust is produced in supernova explosions, the composition of a particular dust grain could be isotopically and chemically different from the interstellar gas in which it is found, which will tend to be well mixed. It may also be that the average composition of the dust differs from that of the gas.

The other two components are related to a recent supernova that may be needed to explain the ^{26}Mg anomaly. There are two possibilities for the existence of ^{26}Al, which seems to be responsible for the ^{26}Mg anomaly. The first explanation for the production of ^{26}Al may be irradiation in the early solar system (Schramm 1971). However, Schramm (1977) has calculated the energy required for this mechanism to produce the observed amount of ^{26}Al, in a manner similar to that used by Ryter *et al.* (1971) for irradiation-produced Li, Be, and B. If the irradiation takes place through a 1 $M_\odot$ cloud of solar composition, then an energy of the order of the binding energy of the Sun is needed, which seems to be unreasonably large. Furthermore, this amount of irradiation would be likely to produce other, so far unseen, anomalies in ^{50}V, ^{40}K, and Gd isotopes (see Schramm 1971; Clayton, Dwek, and Woosley 1977) unless very stringent conditions on the duration and spatial localization of this irradiation are introduced.

A more likely explanation is that one or more supernovae occurred near the protosolar cloud within the interval $\Delta \sim 10^6$ yr of the condensation of the solar system. The ^{26}Al could have been produced by explosive carbon burning or perhaps by high-temperature shell carbon burning. In either case it would be ejected in the supernovae. A final supernova would lead to addition of the two other components, "last-event" gas and dust to the pre–solar-system material. In fact the supernova's expanding shock front, upon encountering the protosolar cloud, may trigger its collapse (Cameron 1962; Cameron and Truran 1976; Woodward 1976; Margolis 1978); Figure 3*b*. Possible observations of this phenomenon have been reported by Herbst and Assousa (1977).

Some mixing of the last-event material with the primordial material occurs at the interface of the shock front with the protosolar cloud. This mixing may be via Rayleigh-Taylor "interfingering" of the gases at the boundary, or it may be via the "shrapnel"-like grains of the supernova penetrating into the protosolar cloud while the bulk of the supernova-produced gas merely passes around it (Fig. 3*c*).

After the passage of the shock front, we assume that the resulting collapse of the protosolar cloud leads to the formation of a "solar nebula" in which pressures and temperatures rise to the ranges suggested by Cameron and Pine (1973). The condensation of the bulk of solar-system matter proceeds as the gas cools.

In order to determine which preexisting grains survive this stage, we will focus our attention on two regions. The first is at a total pressure of 10^{-3} atm and has solar composition (Cameron 1973). The second has the same total pressure, but its composition differs from the first in that its C abundance has been raised such that its C/O ratio is 1.5.

The first region is suitable for the condensation of many of the components of carbonaceous chondrites. Under equilibrium conditions, the only presolar grains which can survive are those which appear in the condensation sequence for solar composition at 10^{-3} atm (see Table 3). Because we are interested in the origin of isotopic anomalies found in Ca-rich inclusions in the Allende meteorite, we will first focus attention on the maximum temperature, T_{max}, reached in their formation location. T_{max} must have been greater than the condensation temperature of forsterite, 1430 K, because the bulk chemical compositions of the inclusions are similar to that calculated for the preforsterite condensate and dramatically different from that for the postforsterite condensate. T_{max} must have been less than the condensation point of corundum, 1742 K, because the magnitude of the oxygen isotope anomalies suggests that a fraction of at least one major oxygen-containing phase survived. From Table 3, there are only five phases which are stable in the temperature range 1742–1435 K. Thus the only presolar condensates of the abundant elements which could have survived are corundum, perovskite, melilite, spinel, and diopside.

Five different cases immediately present themselves. The first is that T_{max} was greater than 1680 K, so that only corundum grains survived. The second occurs if T_{max}, instead, was between 1625 and 1680 K, so that both perovskite and melilite survived, and so on for the other three cases. These grains will contain isotopic anomalies indicative of the supernova zone from which they condensed. These five cases can be combined with the conclusions regarding isotope production of § V and the condensation sequences of § IV. The results are displayed in Table 9. It should be kept in mind that only general trends are indicated. Details depend on the stellar mass, and the physical conditions in the explosive burning stage and in the static burning stages preceding the explosion. It is notable that all these minerals, especially melilite, spinel, and diopside, may be very rich sources of isotopic anomalies.

Consider now a region of the presolar nebula in which the C/O ratio was greater than unity, as seems to be required by the mineralogical composition of enstatite chondrites (Larimer 1975). Since the condensation sequence is so different from the case where C/O < 1, a different suite of presolar minerals could have survived in such a region. The condensation sequence at 10^{-3} atm total pressure for C/O = 1.5 will be very similar to that of the expanding solar zone (Table 4, C/O = 1.5). Unfortunately, no upper or lower limits for T_{max} can be set for enstatite meteorites, since much less is known about their mineralogical history. Thus we will assume, for the sake of argument, that T_{max} was greater than 1193 K, the condensation temperature of corundum. The following six phases could then have survived: TiC, C, SiC, Fe_3C, AlN, and CaS. These six possibilities are summarized in Table 10. Enstatite chondrites may thus prove to be a successful hunting ground for isotopic anomalies in C, Fe, N, S, Ti, Al, and Ca. The isotopic composition of C in certain phases of these meteorites may be a key indicator of which supernova

TABLE 9

SURVIVING GRAINS AND THEIR ANOMALIES IN THE PRESOLAR NEBULA (C/O < 1)

MINERAL T_{cond}	ELEMENT	ZONE (H) C/O < 1	(H) C/O > 1	(He) C/O < 1	(He) C/O > 1	(C) C/O < 1	(C) C/O > 1	(O) S-, Si-poor	(O) S-, Si-rich
Corundum....	O	17+*	17+	17−* 18?*	17− 18?	16+	16+	16+	16+
1742	Al	...	...	...	...	26+	26+	...	...
Perovskite....	O	17+	...	17− 18?	...	16+	...	16+	...
1680	Ca	...	†	‡	†	†	†	40+ 42+	†
	Ti	...	...	‡	...	†	...	46+	...
Melilite.....	O	17+	...	17− 18?	...	16+	...	16+	16+
1625	Mg	...	...	‡	...	25? 26?	...	24+	24+
	Al	...	†	...	†	26+	†	...	...
	Si	...	...	‡	...	29+ 30?	...	28+	28+
	Ca	...	...	‡	...	†	...	40+ 42+	40+ 42+
Spinel.....	O	17+	17+	17− 18?	17− 18?	16+	16+	...	...
1530	Mg	...	...	‡	‡	25? 26?	25? 26?	‡	‡
	Al	...	...	...	...	26+	26+	...	...
Diopside.....	O	17+	17+	17− 18?	17− 18?	16+	16+	16+	16+
1435	Mg	...	...	‡	‡	25? 26?	25? 26?	24+	24+
	Si	...	...	‡	‡	29+ 30?	29+ 30?	28+	28+
	Ca	...	...	‡	‡	‡	‡	40+ 42+	40+ 42+

* A plus indicates possible enhancement of this isotope relative to other stable isotopes and solar abundances; a minus indicates possible depletion of this isotope relative to other stable isotopes and solar abundances; a question mark indicates uncertainty in relative production of this isotope.

† Does not condense in this zone.

‡ Possible enhancement of neutron-rich isotopes due to neutron capture.

TABLE 10

SURVIVING GRAINS AND THEIR ANOMALIES IN THE PRESOLAR NEBULA (C/O > 1)

MINERAL T_{cond}	ELEMENT	ZONE (H) C/O < 1	(H) C/O > 1	(He) C/O < 1	(He) C/O > 1	(C) C/O < 1	(C) C/O > 1	(O) S-, Si-poor	(O) S-, Si-rich
TiC	C	†	13+*	†	13−	†	12+	†	†
1910	Ti	...	...	...	‡	...	‡	...	...
C	C	†	13+	†	13−	‡	12+	†	†
1845	...	...	...	...	...	...	...	...	...
Sic	C	†	13+	†	13−	†	12+	...	...
1745	Si	...	...	...	‡	...	29+ 30?	†	†
Fe_3C	C	†	13+	†	13−	†	12+	†	†
1458	Fe	...	...	...	‡	...	‡	...	...
AlN	N	†	15?	†	15?	†	†	†	†
1400	Al	...	...	...	...	...	...	...	...
CaS	S	†	...	†	‡	†	‡	36−	36−
1390	Ca	...	...	...	‡	...	‡	40+ 42+	40+ 42+

* A plus indicates possible enhancement of this isotope relative to other stable isotopes and solar abundances; a minus indicates possible depletion of this isotope relative to other stable isotopes and solar abundances; a question mark indicates uncertainty in relative production of this isotope.

† Does not condense in this zone.

‡ Possible enhancement of neutron-rich isotopes due to neutron capture.

zones were sampled. A higher $^{13}C/^{12}C$ ratio than the solar one could have originated in an (H) zone, while a lower $^{13}C/^{12}C$ ratio than solar may have stemmed from a (He) or (C) zone.

Tables 9 and 10 enable one to make predictions concerning not only which mineral phases in presolar grains should contain excess ^{26}Mg and excess ^{16}O, among other isotopic peculiarities, but also what other isotopic anomalies should accompany any given anomaly. For example, the existence of both excess ^{26}Mg and ^{16}O in Allende Ca-rich inclusions may be due to Al- and O-rich grains condensed in the O-rich (C) zone. If so, Table 9 predicts that neutron-rich isotopes of Ca and Ti may also be in excess in these inclusions if neutron capture was important in the static helium and explosive carbon-burning zone. In addition, the ratios $^{29}Si/^{28}Si$ and possibly $^{30}Si/^{28}Si$ could have larger than solar values in these inclusions. As another example, suppose that excess ^{24}Mg is also discovered in Ca-rich inclusions. From Table 9, it is seen that grain condensation in the (O) zone could lead to this possibility. One could then further predict that excess ^{28}Si, ^{40}Ca, and ^{42}Ca should also be observable.

One other set of physical conditions in the presolar nebula should be considered. Type 1 carbonaceous chondrites probably condensed under conditions of extremely low temperature $T_{max} \lesssim 400$ K (Grossman 1975). Many presolar mineralogical species may have survived this environment, thus preserving isotopic anomalies in many elements. Unfortunately, thermodynamic data for many low temperature species are unavailable, so the necessary condensation calculations have not as yet been performed. It should be noted that the ^{22}Ne anomaly is found in C1 chondrites.

We note that it may be easier to produce isotopic anomalies with grains than with supernova gas because (1) grains may penetrate to the interior of the protosolar cloud more efficiently than supernova gas, and (2) gas mixing time scales are relatively rapid. To produce nonradiogenic isotopic anomalies with supernova gas requires meteoritic condensation to occur before the complete mixing of supernova gas with nebular gas.

VII. INTERPRETATION OF THE OBSERVED ISOTOPIC ANOMALIES

The ^{16}O anomaly is found in the anhydrous phases of C2 and C3 chondrites. Clayton *et al.* (1977) have found the anomaly to be contained in at least three phases in the Ca-rich inclusions of Allende: spinel, a diopsidic pyroxene rich in Al and Ti, and melilite. They have further determined that the spinel and pyroxene invariably contain larger amounts of excess ^{16}O than the melilite of these inclusions, by about a factor of 4. From textural (Blander and Fuchs 1975) and trace-element (Grossman and Ganapathy 1976*a*) arguments, it appears that Ca-rich inclusions were at least partially melted during or after the condensation process. Melts may exchange atoms or molecules with the ambient gas much more easily than solid phases. As a result, if the isotopic compositions of the condensed phases and the gas differ, mineral phases which subsequently crystallize from the melt may contain different isotopic compositions than those phases which have not been melted. In our scenario, supernova gas mixing with presolar gas at the boundary of the protosolar cloud could lead to isotopic composition gradients across the presolar nebula. Thus the Ca-rich inclusions may have formed in nebular regions with different isotopic composition.

In Ca-rich inclusions, spinel and pyroxene have higher melting temperatures than melilite and anorthite (Seitz and Kushiro 1974). The partial melting of these inclusions could then explain the observed distribution of oxygen isotopes among these phases. There are several ways in which this could have occurred. If grains are responsible for the anomaly, all the original solar nebula condensate phases in the inclusion could

have the same fraction of exotic material. After melting, the lower-melting-point phases would show smaller excesses of ^{16}O if the ambient gas now had a more nearly solar oxygen composition than the inclusion. Alternatively, much or all of the oxygen anomaly could have been due to inclusion condensation in a nebular region in which the proportion of last-event supernova gas was relatively large. Then melting could have later occurred in a nebular region with more nearly solar isotopic abundances. Finally, melting may have been part of the original condensation process, with the time difference between the crystallization of different phases large compared with the time required for changes in the nebular gas composition. In these ways the lower-melting-point phases would contain lesser quantities of anomalous oxygen.

It appears that rare-earth elements in Ca-rich inclusions no longer reside in the phases which carried them into the inclusions (Grossman and Ganapathy 1976*a*). Why the rare earths have been redistributed among all these phases, and not just those with low melting temperatures, as seems to be the case for the oxygen anomaly, remains a mystery. It is hoped that future observations will clarify this problem.

It is very striking that the fraction of excess ^{16}O, while varying from phase to phase, is nearly identical in all samples of a given phase, even those taken from different inclusions. This homogeneity is easier to understand on the basis of a gaseous rather than a crystalline source of excess ^{16}O, but only if condensation occurs before the complete mixing of supernova gas with nebular gas. However, if the inclusions were entirely melted during or after their condensation, there is no reason to favor a gaseous origin, since melting would tend to destroy all traces of preexisting grains and homogenize the isotopic composition within a given phase.

Because particles less than a few microns in size have not yet been individually analyzed, it is uncertain whether presolar grains have actually been observed. If presolar grains are responsible for the ^{16}O anomaly, their identity can be found in Table 9. All five minerals listed contain oxygen and are condensed in either the (C) or (O) zones and hence could contain excess amounts of ^{16}O. The ratio of (corundum + spinel) to (melilite + diopside) condensed in grains in the (C) or (O) zones is approximately equal to the Al/Ca ratio, since this ratio is either much greater than one [(C) zone] or much less than one [(O) zone]. However, the stoichiometry of the minerals in the inclusions does not permit only Al-rich or only Ca-rich carriers of excess ^{16}O. Thus partial or total melting of the inclusions is required, or else the (C) and (O) zones contributed comparable amounts of excess ^{16}O-bearing grains to the solar nebula.

The ^{26}Mg anomaly is also found in these Ca-rich inclusions. Lee, Papanastassiou, and Wasserburg (1977) found the coexisting phases spinel, fassaite (a diopsidic pyroxene), melilite, and anorthite in a single inclusion plot on an Al-Mg isochron, i.e., there is a positive linear correlation between excess ^{26}Mg and the Al/Mg ratio. This implies that the excess ^{26}Mg is the in situ decay product of ^{26}Al. The fact that the ^{26}Mg anomaly has not been detected in other phases of C2 and C3 meteorites is not surprising, since the Mg/Al ratio in these phases is large enough to mask the excess ^{26}Mg. The production ratio of $^{26}Al/^{27}Al$ in the (C) zone is greater than the primordial ratio deduced for the inclusions (Lee, Papanastassiou, and Wasserburg 1977), as it should be. Table 9 indicates that presolar grains of corundum, melilite, or spinel could have been carriers of ^{26}Al.

It could be argued that the major phases of the inclusions condensed from the solar nebula and incorporated tiny supernova condensate grains containing either live ^{26}Al or its decay product ^{26}Mg, but this would call for an unbelievable coincidence. The amount of ^{26}Al or excess ^{26}Mg incorporated by the phases would have had to be directly proportional to their known Al/Mg ratio. There seems to be no *a priori* reason for such a phenomenon. If the data define a perfect isochron and if the ^{26}Al has a supernova origin, there are two possible explanations. All phases of the inclusions could have condensed from the vapor with the same $^{26}Mg/^{24}Mg$ ratio and different $^{26}Al/^{24}Mg$ ratios. Alternatively, all these phases could have crystallized from or equilibrated with the melt, each obtaining the same $^{26}Mg/^{24}Mg$ ratio and a different $^{26}Al/^{24}Mg$ ratio, thus obliterating any prior evidence relating to the question of whether the source of the ^{26}Al was gaseous or crystalline. That the higher- and lower-melting-point phases have different contents of excess ^{16}O but not ^{26}Mg could be due to the relative diffusion rates in these minerals of oxygen and the cations magnesium and aluminum, which are not now known.

What if the data do not define a perfect isochron? The fact that the higher-melting-point phases spinel and fassaite have such small Al/Mg ratios means that small deviations from the isochrons, within experimental error, could imply relatively large differences in their initial $^{26}Al/^{27}Al$ ratios. If the initial system was closed, i.e., if no isotopic exchanges with the ambient gas took place after initial condensation, an imperfect isochron could result if partial melting occurred. This happens regardless of whether the initial system had a homogeneous distribution of the $^{26}Mg/^{24}Mg$ and $^{26}Al/^{27}Al$ ratios or a heterogeneous distribution. The latter would be due to different minerals containing different amounts of ^{26}Mg- and/or ^{26}Al-bearing grains, or condensing in different nebular regions. If the system was, on the other hand, open, then the initial system could have been either homogeneous or heterogeneous; the result would be an imperfect isochron unless complete melting occurred. For example, as in the case of the oxygen anomaly, the melting of only the lower-melting-point phases melilite and or anorthite could homogenize their $^{26}Al/^{27}Al$ and $^{26}Mg/^{24}Mg$ ratios, but not those of the higher-melting-point phases spinel and fassaite, which might originally have contained different ratios. Alternatively, Clayton and Mayeda (1977) have suggested that the ^{26}Al was initially introduced into the inclusions during the melting process by exchange

with injected supernova gas, so that only the lower-melting-point phases melilite and anorthite would contain appreciable quantities of ^{26}Al, as is observed.

A grain origin for the ^{22}Ne anomaly would be possible, if the meteorites in which it is found (C1 chondrites) were formed with peak temperatures of at most ~400 K, as argued by Grossman (1975). The 2.6 yr ^{22}Na could be produced in the (He) zone and condensed into a sodium-bearing mineral, such as $NaAlSi_3O_8$ (see Table 4). If the decay-produced ^{22}Ne can be retained in or on these grains at 400 K, incorporation of excess ^{22}Ne into C1 chondrites may occur (see also Clayton 1975*b*; Sabu and Manuel 1976). However, irradiation in the early solar nebula could also produce excess ^{22}Ne (Black 1972). The energy requirements are much less stringent than for the production of ^{26}Mg by irradiation, so other isotopic anomalies may not be produced simultaneously.

Let us now consider the meaning of the difference between the time scales implied by aluminum and by xenon. Schramm and Wasserburg (1970) have determined that the interval between the production of the *r*-process parent of Xe and the trapping of Xe in meteorites is about 10^8 yr. On the other hand, the Al time scale is of the order of the half-life of ^{26}Al, assuming the anomalous ^{26}Mg is interpretable as the in situ decay product of ^{26}Al. If the Al and Xe were produced in the same event, these time scales are in apparent disagreement. At least two explanations seem available.

First, suppose that Al and Xe were produced in separate nucleosynthetic events. The heavy isotopes of Xe are daughter nuclei of *r*-process parent nuclei (^{129}I, ^{244}Pu). An *r*-process event may have occurred in the vicinity of the presolar material on its last passage through a spiral arm, setting the zero point of the Xe retention time scale. Then, with the next passage of a spiral arm, 10^8 yr later, came the star formation and the subsequent supernova that may have triggered the collapse of the presolar nebula. Perhaps this supernova was not an *r*-process source, but did produce ^{26}Al. It may be that *r*-process sources are relatively rare. In this scenario, formation of the meteorites, and retention of both Al and Xe, occurred 10^6 yr later.

A second explanation assumes that both Al and Xe were produced in the same supernova, 10^6 yr before the meteorites condensed. Perhaps the nebular regions where meteorites or the meteorite parent bodies themselves formed remained too hot, for 10^8 yr, for Xe to be trapped.

A search for ^{235}U anomalies due to the decay of ^{247}Cm (Blake and Schramm 1973) might help one choose between these explanations. Curium-247 is *r*-process produced, as are ^{129}I and ^{244}Pu, two parents of Xe with half-lives of 1.7×10^7 yr and 8.3×10^7 yr, and has a half-life of 1.54×10^7 yr. If the ^{235}U time scale turned out to be of the order of 10^8 yr, the former explanation would be strongly favored, since uranium does not have the mobility of xenon.

The origin of the anomalous xenon isotopes (Lewis, Srinivasan, and Anders 1975; Sabu and Manuel 1977) remains uncertain. It is possible that the anomaly in the heavy Xe isotopes could be due to an *r*-process superheavy element as proposed by Anders and Heymann (1969). The anomaly in the light isotopes could be due to a supernova *p*-process or to isotopic fractionation. In situ decay of the superheavy element in the same grains that contained the light xenon isotopes then occurred. However, that is not to say that other scenarios could not be drawn. To adequately interpret this problem, one needs a better understanding of the mineral "Q" (Lewis, Srinivasan, and Anders 1975) and an experimental separation of the light and heavy xenon isotopes.

It is interesting that no isotopic anomalies have been observed in the very refractory elements osmium (Grossman and Ganapathy 1976*b*; Takahashi *et al.* 1976) and calcium (Lee, Papanastassiou, and Wasserburg 1977). Perhaps the last-event supernova did not synthesize anything beyond explosive carbon burning. An alternative is that only supernova shells down to the (C) zone were able to mix with the protosolar cloud; interior zones [(O), (Si), and *r*-process] from this last event were not incorporated into the solar system. Clearly, further experimental study regarding heavy-element anomalies is needed before anything definitive can be stated.

VIII. CONCLUSIONS

An "onionskin" presupernova model has been used to estimate the chemical and isotopic abundance in the various shells of ejected supernova material. Condensation calculations have been performed over a range of pressures and chemical compositions for each of these shells in order to determine the possible grains that could be produced in supernova ejecta. Employing a four-component model of the presolar nebula, we have emphasized the distinction between "old" supernova grains and "last-event," or "new," supernova grains. The existence of this last-event supernova may be necessary to account for the ^{26}Mg isotopic anomaly. There may also be a difference between interstellar gas, which has been enriched by supernova debris throughout galactic history, and last-event supernova gas.

This paper has investigated the type of grains which might be produced in a supernova. An interesting future project might be to consider this grain source with grains produced in novae, red giants, etc., coupled with interstellar destruction mechanisms to theoretically follow the evolution of interstellar grain composition.

Only grains that are stable under the physical conditions encountered in the presolar nebula can survive and retain their anomalous composition. Two regions in the presolar nebula are considered, and the possible surviving grains are deduced from the appropriate condensation sequences. In regions of solar composition and peak temperatures in the range 1430–1755 K, which gave rise to the Ca-rich inclusions found in C3 chondrites, corundum, perovskite, melilite, spinel,

and diopside are candidates for presolar grains. If the C/O ratio was, instead, greater than 1, TiC, C, SiC, Fe_3C, AlN, and CaS may survive. This region corresponds to the conditions thought to be necessary for enstatite chondrites to form. Each of these minerals is produced in one or more supernova zones.

The ^{16}O anomaly has been found in the Ca-rich inclusions of C3 chondrites, in the minerals spinel, pyroxene, and melilite. This anomaly could be explained by the incorporation of gas or grains into these inclusions from the (C) and (O) zones in which large ^{16}O excesses are expected. The distribution of excess ^{16}O among the various mineral phases in these inclusions could be explained by the partial melting of these inclusions. In the absence of any melting, the homogeneous isotopic composition of a given phase in different inclusions argues in favor of a gaseous origin rather than a granular origin for the oxygen anomaly.

The ^{26}Mg anomaly has been found to be correlated with the aluminum abundance in Ca-rich inclusions Allende, which implies that it is the in situ decay product of ^{26}Al. Explosive carbon-burning calculations show the production ratio of $^{26}Al/^{27}Al$ to be consistent with the ratio deduced from the observations of Lee *et al.* However, high-temperature shell carbon burning immediately preceding the supernova may produce a similar $^{26}Al/^{27}Al$ ratio. If the observational data define a perfect isochron, either all the phases in the inclusion condensed from the vapor, or else these phases crystallized from or equilibrated with a melt. But the quoted uncertainties in the data for the higher-melting-point phases, the relative smallness of their Al/Mg ratio and excess ^{26}Mg content, and the lack of information concerning their original $^{26}Mg/^{24}Mg$ ratio may, in fact, mean that the higher-melting-point phases do not lie on an isochron with the lower-melting-point phases.

The ^{22}Ne anomaly may be produced by irradiation in the early solar system, or by presolar grains that originally contained ^{22}Na. These grains cannot have been subjected to high temperatures (> 1000 K), or they would have vaporized. This is consistent with textural and chemical arguments which suggest that C1 chondrites, in which excess ^{22}Ne is found, may have formed in nebular regions whose peak temperatures did not exceed 400 K.

The difference between the retention time scales of Xe (10^8 yr) and Al (10^6 yr) may be due to the fact that the *r*-process progenitors were present in the presolar nebula only in the interstellar gas and/or dust components, which had been last enriched about 10^8 yr before. On the other hand, the anomalous aluminum may have been produced in the last-event supernova 10^6 yr before the inclusions condensed. Another possibility is that both are last-event products, but that somehow the xenon was unable to be retained in the meteorites until 10^8 yr after nucleosynthesis.

The lack of anomalies in Os and Ca may indicate that the last-event supernova did not synthesize anything beyond explosive carbon burning, or that matter interior to this zone did not enter the presolar nebula.

We would like to acknowledge valuable discussion on this subject with E. Anders, D. Arnett, R. N. Clayton, S. Colgate, S. Falk, and J. Truran. One of us (J. M. L.) expresses his appreciation for the hospitality of the Institute of Astronomy, Cambridge, England, and NORDITA, Copenhagen, Denmark, where part of this research was done. This work was supported in part by NSF grants AST 73-05117 and AST 76-22673 at the University of Illinois (J. M. L.), and AST 74-21216 and AST 76-21707 at the University of Chicago (J. M. L. and D. N. S.), by NASA grants NGR 14-001-249 (L. G.) and NSG 7212 (J. M. L. and D. N. S.) at the University of Chicago, and by the Alfred P. Sloan Foundation (L. G.).

APPENDIX

In this Appendix the effect of radioactive heating upon the expanding supernova shells is estimated. Assuming the material to be homogeneous, the first law of thermodynamics gives

$$\frac{dQ}{dt} = \frac{dE}{dt} + P\frac{dV}{dt},$$

where

$$E = \tfrac{3}{2}NkT + aT^4V; \qquad P = P_g + P_r = \frac{N}{V}kT + \tfrac{1}{3}aT^4.$$

E is the internal energy, P the pressure, V the volume, T the temperature, and P_g and P_r are the gaseous and radiation pressure, respectively. If the matter is spherically symmetric with radius R and expanding uniformly with velocity v, then

$$\frac{1}{V}\frac{dV}{dt} = \frac{3v}{R} = 3\frac{dR}{Rdt} = -\frac{dT}{T(\gamma - 1)dt}, \tag{A1}$$

which defines the effective adiabatic exponent γ. When the above three equations are combined, γ is found to be

$$\gamma = \left(-\frac{dQ}{dt}\frac{R}{3vV} + 16P_r + \tfrac{5}{2}P_g\right)\Big/(12P_r + \tfrac{3}{2}P_g).$$

We consider explicitly the most important case of radioactivity, that of the two-step β-decay $^{56}\mathrm{Ni} \rightarrow {}^{56}\mathrm{Co} \rightarrow {}^{56}\mathrm{Fe}$. For simplicity it is assumed that each decay releases $\epsilon \approx 1$ MeV of energy that is immediately thermalized in the expanding cloud. The two decay half-lives of ^{56}Ni and ^{56}Co are $\tau_{\mathrm{Ni}} = 6$ days $\sim 5 \times 10^5$ s and $\tau_{\mathrm{Co}} = 77$ days $\sim 6.3 \times 10^6$ s, respectively. If n_{Ni}, n_{Co}, and n_{Fe} represent the number density of each isotope, then

$$n_{\mathrm{Ni}}(t) + n_{\mathrm{Co}}(t) + n_{\mathrm{Fe}}(t) = fN = n_{\mathrm{Ni}}(0); \qquad n_{\mathrm{Co}}(0) = n_{\mathrm{Fe}}(0) = 0,$$

and

$$\frac{dQ}{dt} = -\epsilon \frac{dn_{\mathrm{Ni}}}{dt} + \epsilon \frac{dn_{\mathrm{Fe}}}{dt}, \tag{A2}$$

where f is the number fraction of Ni nuclei initially in the expanding matter. It is straightforward to show that equation (A2) may be written as

$$\frac{dQ}{dt} = \frac{\epsilon f N}{(\tau_{\mathrm{Co}} - \tau_{\mathrm{Ni}})} \left[e^{-t/\tau_{\mathrm{Ni}}} \left(\frac{\tau_{\mathrm{Co}}}{\tau_{\mathrm{Ni}}} - 2 \right) + e^{-t/\tau_{\mathrm{Co}}} \right]. \tag{A3}$$

The time t is given simply by $t = [R - R(0)]/v$.

The differential equation (A1) has been integrated for the initial conditions $R(0) = 10^8$ cm, $v = 10^8$ cm s^{-1}, $T(0) = 4 \times 10^9$ K, $f = 0$, and the density $\rho(0) = 10^5$ g cm^{-3}; these conditions are such that radiation pressure is initially dominant. The results are shown by the $f = 0.0$ line in Figure 1. Also plotted are the results of changing f; changing R and v change only the time scale. It is apparent that if $f = 10^{-5}$, the density at 2000 K is about a hundred times less than the nonradioactive ($f = 0$) case. If $f = 0.5$, the ratio of densities is less than 10^{-5}.

The effect is even more pronounced if the initial conditions are such that gas pressure dominates. Figure 2 displays the integrations for the same initial conditions, except now $T(0) = 10^9$ K, for a variety of values of f. The ratio of the final densities for the cases $f = 0.5$ and $f = 0$ is about 10^{-14}. Note that the rapid initial cooling of the matter enables the radioactive heat input to actually increase the temperature after several days. The case $f = 10^{-5}$ is especially interesting, since the temperature apparently falls low enough to permit grain formation before rising again to such a high value that the grains would surely evaporate. By the time the temperature again reaches a few thousand degrees, the density is 10 orders of magnitude less than it was when the matter initially condensed. Condensation might now be impossible.

Finally, the effect of luminosity losses has been estimated by the use of an effective radiative temperature T_{rad}, which is defined to be equal to T or 10^4 K, whichever is less. Equation (A3) is modified, and now contains the additional term $-\pi R^2 a c T_{\mathrm{rad}}^4$. The simplicity of this approximation is evident in the dotted trajectories in Figures 1 and 2, which show dramatic decreases in temperature near 10^4 K when radiation pressure dominates. Nevertheless, had radiative transfer been more accurately treated, the results would still show the loss of internal energy at low temperatures when radiation pressure dominates.

REFERENCES

Anders, E., and Heymann, D. 1969, *Science*, **184**, 821.
Arnett, W. D. 1969, *Ap. J.*, **157**, 1369.
———. 1973, in *Explosive Nucleosynthesis*, ed. D. N. Schramm and W. D. Arnett (Austin: University of Texas Press), p. 236.
———. 1977, preprint.
Arnett, W. D., and Schramm, D. N. 1973, *Ap. J. (Letters)*, **184**, L47.
Black, D. C. 1972, *Geochim. Cosmochim. Acta*, **36**, 377.
Black, D. C., and Pepin, R. O. 1969, *Earth Planet. Sci. Letters*, **6**, 395.
Blake, J. B., and Schramm, D. N. 1973, *Nature Phys. Sci.*, **243**, 138.
Blander, M., and Fuchs, L. H. 1975, *Geochim. Cosmochim. Acta*, **39**, 1605.
Cameron, A. G. W. 1962, *Icarus*, **1**, 13.
———. 1968, in *Origin and Distribution of the Elements*, ed. L. H. Ahrens (London: Pergamon Press), p. 125.
———. 1973, in *Explosive Nucleosynthesis*, ed. D. N. Schramm and W. D. Arnett (Austin: University of Texas Press), p. 3.
Cameron, A. G. W., and Pine, M. R. 1973, *Icarus*, **18**, 377.
Cameron, A. G. W., and Truran, J. W. 1976, *Icarus*, **30**, 447.
Chevalier, R. 1976, *Ap. J.*, **207**, 872.
Clayton, D. D. 1975*a*, *Ap. J.*, **199**, 765.
———. 1975*b*, *Nature*, **257**, 36.
Clayton, D. D., Dwek, E., and Woosley, S. E. 1977, *Ap. J.*, **214**, 300.
Clayton, D. D., and Hoyle, F. 1976, *Ap. J.*, **203**, 490.
Clayton, R. N., Grossman, L., and Mayeda, T. K. 1973, *Science*, **182**, 485.
Clayton, R. N., and Mayeda, T. K. 1977, *Geophys. Res. Letters*, **4**, No. 6.
Clayton, R. N., Onuma, N., Grossman, L., and Mayeda, T. K. 1977, *Earth Planet. Sci. Letters*, **34**, 209.
Couch, R. G., Schmeidekamp, A. B., and Arnett, W. D. 1974, *Ap. J.*, **190**, 95.
Eberhardt, P. 1974, *Earth Planet. Sci. Letters*, **24**, 182.
Falk, S., and Arnett, W. D. 1977, *Ap. J. Suppl.*, **33**, 515.
Falk, S., and Scalo, J. M. 1975, *Ap. J.*, **202**, 690.
Feder, J., Russell, K. C., Lothe, J., and Pound, G. M. 1966, *Adv. Phys.*, **15**, 11.
Fix, J. D. 1969, *M.N.R.A.S.*, **146**, 37.
Gray, C. M., and Compston, W. 1974, *Nature*, **251**, 495.
Grossman, L. 1972, *Geochim. Cosmochim. Acta*, **36**, 597.
———. 1975, *Sci. Am.*, **232**, 30.
Grossman, L., and Ganapathy, R. 1976*a*, *Geochim. Cosmochim. Acta*, **40**, 331.
———. 1976*b*, *EOS Trans. AGU*, **57**, 278.
Hainebach, K. L., Norman, E. B., and Schramm, D. N. 1976, *Ap. J.*, **203**, 245.
Herbst, W., and Assousa, G. E. 1977, preprint.
Howard, W. M., Arnett, W. D., and Clayton, D. D. 1971, *Ap. J.*, **165**, 495.
Hoyle, F., and Wickramasinghe, N. 1970, *Nature*, **226**, 62.
Joint Army Navy Air Force (JANAF) Thermochemical Tables. 1960, and later supplements.
Kantrowitz, A. 1951, *J. Chem. Phys.*, **19**, 1097.
Lamb, S. A., Howard, W. M., Truran, J. W., and Iben, I. 1977, preprint.
Larimer, J. W. 1968, *Geochim. Cosmochim. Acta*, **32**, 1187.

Larimer, J. W. 1975, *Geochim. Cosmochim. Acta*, **39**, 389.
Larimer, J. W., and Bartholomay, M. 1976, preprint.
Lee, T., and Papanastassiou, D. A. 1974, *Geophys. Res. Letters*, **1**, 225.
Lee, T., Papanastassiou, D. A., and Wasserburg, G. J. 1977, *Ap. J. (Letters)*, **211**, L107.
Lewis, R. S., Srinivasan, B., and Anders, E. 1975, *Science*, **190**, 1251.
Margolis, S. 1978, in preparation.
Pardo, R. C., Couch, R. G., and Arnett, W. D. 1974, *Ap. J.*, **191**, 711.
Robie, R. A., and Waldbaum, D. R. 1968, U.S.G.S. Bull, No. 1259.
Ryall, W. R., and Muan, A. 1969, *Science*, **165**, 1363.
Ryter, C., Reeves, H., Gradsztajn, E., and Audouze, J. 1971, *Astr. Ap.*, **8**, 389.
Sabu, D. D., and Manuel, O. K. 1976, *Nature*, **262**, 28.
———. 1977, preprint.
Salpeter, E. E. 1974, *Ap. J.*, **193**, 579.
Schramm, D. N. 1971, *Ap. Space Sci.*, **13**, 249.
———. 1977, *Bull. AAS*, **9**, 454.
Schramm, D. N., and Arnett, W. D. 1975, *Mercury*, **4**, 16.
Schramm, D. N., and Wasserburg, G. J. 1970, *Ap. J.*, **162**, 57.
Seitz, M. G., and Kushiro, I. 1974, *Science*, **183**, 954.
Takahashi, H., Higuchi, H., Gros, J., Morgan, J. W., and Anders, E. 1976, *Proc. Natl. Acad. Sci.*, **73**, 2453.
Thompson, A. B. 1974, *Contrib. Mineral Petrol.*, **48**, 123.
Truran, J. W., and Arnett, W. D. 1970, *Ap. J.*, **160**, 181.
Truran, J. W., and Cameron, A. G. W. 1978, *Ap. J.*, in press.
Woodward, P. R. 1976, *Ap. J.*, **207**, 484.
Woosley, S. E., Arnett, W. D., and Clayton, D. D. 1973, *Ap. J. Suppl.*, **26**, 231.

LAWRENCE GROSSMAN: Enrico Fermi Institute, 5640 S. Ellis Ave., Chicago, IL 60637

JAMES M. LATTIMER: Department of Astronomy, University of Illinois, Urbana, IL 61801

DAVID N. SCHRAMM: Enrico Fermi Institute, Laboratory for Astrophysics and Space Research, 933 E. 56th Street, Chicago, IL 60637